An Algorithm for Interpolating the Frequency Variations of Method-of-Moments Matrices Arising in the Analysis of Planar Microstrip Structures

Junho Yeo, *Student Member, IEEE,* and Raj Mittra, *Life Fellow, IEEE*

***Abstract*—This paper presents a new impedance matrix interpolation algorithm, in the context of method of moments, for planar microstrip structures. Three different interpolating functions are implemented depending upon the distance between the basis and testing functions. To demonstrate its efficiency, the technique is applied to several planar microstrip structures, *viz*. a patch antenna fed by microstrip line and a 4×4 planar patch array. It is demonstrated that the use of the proposed impedance matrix interpolation scheme can result in significant savings in the computation time with little or no compromise in the accuracy of the solution.**

***Index Terms*—Impedance matrix interpolation, method of moments (MoM), microstrip patch antenna, probe-fed square patch array.**

I. Introduction

FIELD solvers based on the method of moments (MoM) are often used for the analysis and design of a wide variety of antennas and arrays since it reduces the problem domain to regions where the surface current densities are defined, thereby reducing the number of unknowns significantly when compared to the finite methods [1]–[4]. Even so, as the problem geometry becomes large, the computation of the MoM impedance matrix elements consumes a considerable portion of the total solution time because this computation requires $O(N^2)$ operations, where N is the number of unknowns, and must be repeated at each frequency. Thus, it is desirable to devise ways by which the computation time for impedance matrix can be shortened, without, of course, sacrificing the accuracy of the solution.

One promising approach to speeding up the time for matrix generation is the impedance matrix interpolation. The concept of the impedance matrix interpolation was first proposed by Newman and Forrai [5] and Newman [6] for the scattering analysis of a microstrip patch and the computation of the impedance of a straight dipole antenna and a flat square plate. Virga and Rahmat-Samii have also applied this technique to evaluate the performance of complex antenna structures designed for personal communications applications [7], [8]. In a follow-up paper, Barlevy and Rahmat-Samii [9], [10] have modified the interpolating function used in [7] and [8] and have applied the new version to predict the response of frequency selective surfaces (FSSs). However, in these papers, the interpolation scheme has been employed only for structures in free space, e.g., freestanding FSSs or antennas, and the performance of this scheme when applied to planar microstrip structures has never been examined.

In this paper, we present a new matrix interpolation scheme and demonstrate its efficacy by analyzing a variety of planar microstrip structures. In this scheme, we begin by computing and storing the impedance matrix elements at three selected frequencies, and then generate them at intermediate frequencies within the band via interpolation. The present interpolation scheme differs from those employed previously in a rather significant way because it uses "different" interpolating functions in three different regions, *viz*. near, intermediate, and far, defined on the basis of the distance between the source and testing functions. To validate the technique, and to illustrate its versatility, the proposed interpolation technique is applied to some typical planar microstrip structures, *viz*. a microstrip line-fed antenna and a 4×4 planar patch array.

II. New Impedance Matrix Interpolation Algorithm

In this section, we summarize the MoM formulation used in this paper and the new impedance matrix interpolation scheme. We begin our discussion by describing the formulation of the MoM for microstrip structures with a single-layer substrate, which is an electric field integral equation (EFIE), and consider that the substrate and ground plane are transversely unbounded with respect to the z-axis [4]. Let us assume that an incident field, generated by a given source, impinges upon the surface of a conducting structure and induces a current distribution $J_S(r)$, which we are trying to solve for by imposing the boundary condition

$$E(r) = Z_S J_S(r), \qquad r \in S \tag{1}$$

where S is the conducting surface, $E(r)$ is the total tangential field on the surface, and Z_S is the surface impedance of the conductor. From the boundary condition associated with the tangential electric field in the surface of the conductor

$$E_i(r) + E_S(r) = Z_S J_S(r) \tag{2}$$

Manuscript received July 29, 2002; revised October 24, 2002.

The authors are with the Electromagnetic Communication Laboratory, Pennsylvania State University, University Park, PA 16802 USA (e-mail: mittra@engr.psu.edu).

Digital Object Identifier 10.1109/TMTT.2003.808703

where $E_i(r)$ is the incident field on the conducting surface, Z_S is the surface impedance of the conductor, and $E_S(r)$ is the scattered field, which can be expressed by an electric scalar potential V and a magnetic vector potential A as

$$E_S(r) = -j\omega A - \nabla V \tag{3}$$

where ω is the angular frequency.

Substituting (3) into (2), we obtain the desired mixed potential integral equation (MPIE)

$$E_i(\rho) = j\omega \int_S ds' \overline{\overline{G_A}}(\rho|\rho') \cdot J_S(\rho') + \nabla \int_S ds' G_V(\rho|\rho') q_S(\rho') + Z_S J_S(\rho) \tag{4}$$

where

$$V(\rho) = \int_S ds' G_V(\rho|\rho') q_S(\rho') \tag{5}$$

$$A(\rho) = \int_S ds' \overline{\overline{G_A}}(\rho|\rho') \cdot J_S(\rho') \tag{6}$$

$\overline{\overline{G_A}}$ and G_V are the Green's functions of the magnetic vector potential and electric scalar potential for microstrip structures, respectively, $\rho = \hat{x}x + \hat{y}y$ is the projection of r on the (x, y) plane, and q_S is a charge density, which is related to the current density through the continuity equation

$$\nabla \cdot J_S + j\omega q_S = 0. \tag{7}$$

Next, we assume that the current distribution is represented by a set of rooftop basis functions as

$$J_S = \sum_n I_n T_n, \qquad n = 1, 2, \ldots, N \tag{8}$$

and the charge density as

$$j\omega q_S = \sum_n I_n \Pi_n, \qquad n = 1, 2, \ldots, N \tag{9}$$

where the x and y components of the current distribution can be expressed separately as

$$J_{Sx} = \frac{1}{\Delta y} \sum_n I_{xn} T_{xn}$$

$$J_{Sy} = \frac{1}{\Delta x} \sum_n I_{yn} T_{yn} \tag{10}$$

$$T_{xn} = \begin{cases} 1 - \dfrac{|x|}{\Delta x}, & |x| < \Delta x \text{ and } |y| < \dfrac{\Delta y}{2} \\ 0, & \text{elsewhere} \end{cases}$$

$$T_{yn} = \begin{cases} 1 - \dfrac{|y|}{\Delta y}, & |x| > \dfrac{\Delta x}{2} \text{ and } |y| < \Delta y \\ 0, & \text{elsewhere} \end{cases} \tag{11}$$

Δx and Δy are x and y-directed current cell size, respectively, and the functions $\prod_n = -\nabla \cdot T_n$ correspond to the pulse doublets.

By applying the Galerkin procedure, we obtain an $N \times N$ matrix equation, which leads

$$[Z_{mn}][I_n] = [V_m] \tag{12}$$

where $[Z_{mn}]$ is the $N \times N$ impedance matrix, $[I_n]$ is the $N \times 1$ current distribution coefficient matrix to be determined, $[V_m]$ is the $N \times 1$ voltage or excitation matrix, and the elements of the impedance matrix are expressed by the contribution of the magnetic vector potential, electric scalar potential, and ohmic losses [4] as

$$z_{mn} = a_{mn} + v_{mn} + l_{mn} \tag{13}$$

$$a_{mn} = j\omega \int_{Sm} ds T_m(\rho) \cdot \int_{Sn} ds' \overline{\overline{G_A}}(\rho|\rho') \cdot T_n(\rho') \tag{14}$$

$$v_{mn} = \frac{1}{j\omega} \int_{Sm} ds \Pi_m(\rho) \int_{Sn} ds' G_V(\rho|\rho') \Pi_n(\rho') \tag{15}$$

$$l_{mn} = Z_S \int_{Sm} ds T_m(\rho) \cdot T_n(\rho'). \tag{16}$$

Equation (12) is solved for the current coefficients by using either a direct or an iterative method, and other quantities of interest, e.g., the S-parameters and radiation pattern, are subsequently derived from the knowledge of this distribution. In this paper, we concentrate on the matrix generation problem as we sweep the frequency, and describe the proposed approach in the following paragraph.

It is a well-known fact that most parameters of interest, such as the induced current distribution and input impedance, exhibit rapid frequency variations caused by resonance characteristics of the circuit. However, the impedance matrix elements are relatively smooth in their behaviors, and it is a better strategy to interpolate them, as has been suggested in some previous papers [6], rather than attempt to do the same with the final solution.

To understand the behavior of the impedance matrix elements for microstrip structures as functions of the frequency, let us consider (14)–(16). In our formulation, the impedance matrix elements of the MoM can be separated into three terms in accordance with their contributions to the matrix elements. The first of these corresponds to the contribution of the magnetic vector potential A and is related to a magnetic vector Green's function $\overline{\overline{G_A}}$. The second one is from the contribution of the electric scalar potential V and is related to the electric scalar Green's function G_V. Finally, the third one is the contribution of the ohmic losses. We note that the frequency variations of the impedance matrix elements are intimately related to those of the above Green's functions, and we take advantage of this fact to postulate the frequency behaviors of the matrix elements. Note that there is a $j\omega$ factor contained in the first term, and a $1/j\omega$ factor in the second term, and these behaviors are reflected in the matrix elements as well. The behaviors of the Green's functions for a microstrip structure have been investigated by many researchers [11]–[13]. It turns out that the magnitude of the vector Green's function changes little with frequency, while the corresponding variation of the scalar Green's function depends on the distance. In the near region, the scalar Green's function varies little with frequency, while its magnitude is proportional to f^2 for the intermediate region, where f is the frequency; also, in the far region, it is proportional to f^4. Hence, we need to use different interpolating functions depending on the distance between the source and testing functions. In the intermediate and far regions, the phase varies rapidly as a function of frequency and needs to be factored out before we begin the interpolation process.

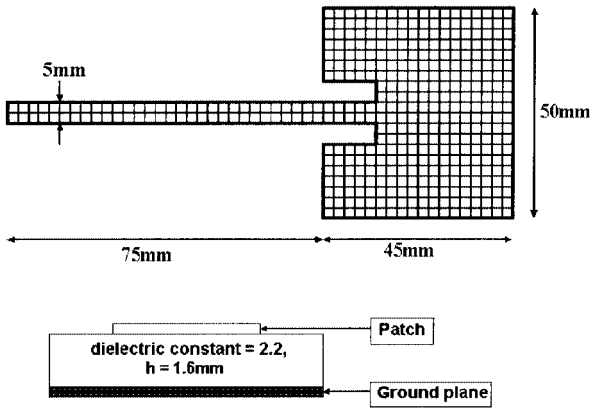

Fig. 1. Geometry of a patch antenna fed by a microstrip line.

When dealing with the free-space Green's function, as in the algorithms in [5]–[10], the normalized distance $k_0 r$ is used to describe its behavior, where k_0 and r are the propagation constant and the distance between the source and testing functions in free space, respectively. However, when working with microstrip-type structures, we need to replace $k_0 r$ with $k_e \rho$, where k_e is the effective wavenumber of the microstrip structure, and ρ is the radial distance in the x–y-plane. Previous workers have used the distance criterion of $0.5\lambda_0$ for free-space structures to factor out the phase term, where λ_0 is the free-space wavelength, because the phase variation is less than 180° $(k_0 r \leq \pi)$ when the distance is less than $0.5\lambda_0$. We have carried out extensive numerical experiments with microstrip structures and have identified the following distance criteria on the basis of these experiments: $\rho_0 = 0.45\lambda_e$ for transitioning from the near to the intermediate region, where λ_e is the effective wavelength, and $\rho_1 = 0.75\lambda_e$ for moving from the intermediate into the far region.

A microstrip line-fed patch antenna, shown in Fig. 1, is considered to illustrate the behavior of the impedance matrix elements as functions of the frequency. Fig. 2 shows the impedance matrix of typical elements of the patch antenna as functions of the frequency, ranging from 1 to 5 GHz, for three different distance cases. The current on the antenna is modeled by using rooftop basis functions and the discretization of the antenna geometry is performed on a uniform rectangular grid. All three elements correspond to those elements for the x-directed rooftop basis and testing functions. For the near region, where the distance between the basis and testing functions is relatively small $(\rho_{mn} < 0.45\lambda_e)$, Fig. 2 shows that the imaginary part of a typical impedance matrix element is much larger than the real part, which decreases inversely as a function of frequency (f^{-1}), and its phase variation is very small. For the intermediate region $(0.45\lambda_e \leq \rho_{mn} \leq 0.75\lambda_e)$, we observe an increase in the magnitude of the real parts of the matrix elements, as well as their phase variations. For the far region $(\rho_{mn} > 0.75\lambda_e)$, the real parts of the impedance matrix now become comparable to the imaginary parts and the phase fluctuates as a function of the frequency.

In the impedance matrix interpolation process, first the matrices at three selected frequencies are directly calculated by

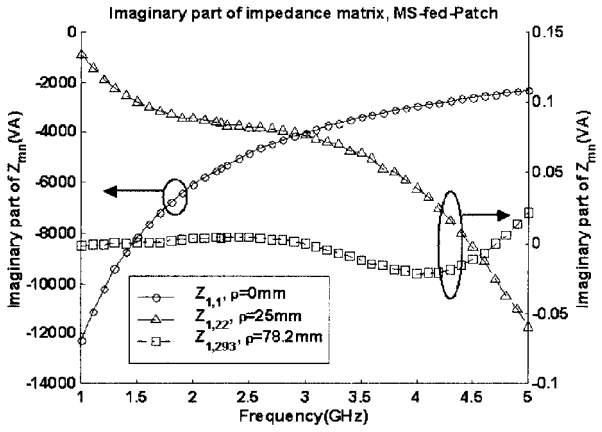

(a)

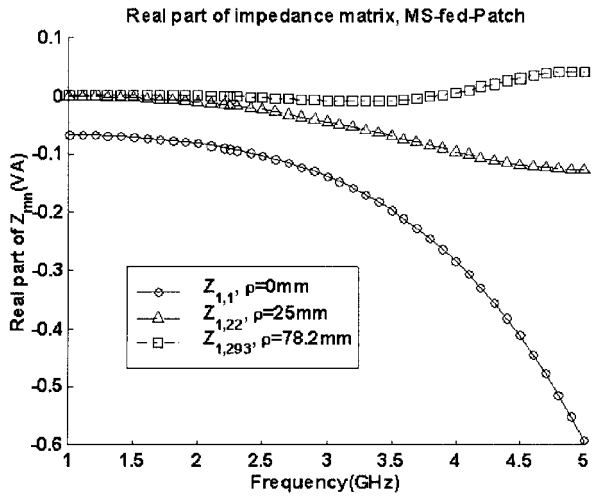

(b)

Fig. 2. Impedance matrix elements of the microstrip line-fed patch antenna for three different distances. (a) Imaginary part. (b) Real part.

using (13), and the results are stored. These matrices are subsequently used to interpolate the elements at the intermediate frequencies. Due to the inherent differences in the behaviors of the matrix elements in the three different regions, *viz*. near, intermediate, and far, we choose different interpolating functions for the imaginary parts of the elements. However, a quadratic interpolating function $(A + Bf + Cf^2)$ is always found to be adequate for the real part over the entire region.

Turning now to the imaginary part, for the near region $(\rho_{mn} < 0.45\lambda_e)$, we interpolate it by using an inverse f function in f^{-1}, which contains both the linear and inverse terms, given by

$$X(f) = A\frac{B}{f} + Cf. \tag{17}$$

To demonstrate its effectiveness, we compare the results of the interpolation using this scheme with two others. We apply all three schemes to the imaginary part of the matrix element $Z_{1,1}$ (self-term) for a patch antenna fed by a microstrip line, the other two being $(A + Bf + Cf^2)$ and $(A + B\ln(f) + Cf)$ functions. A comparison of the interpolation results with the direct computation are shown in Fig. 3(a), with the impedance

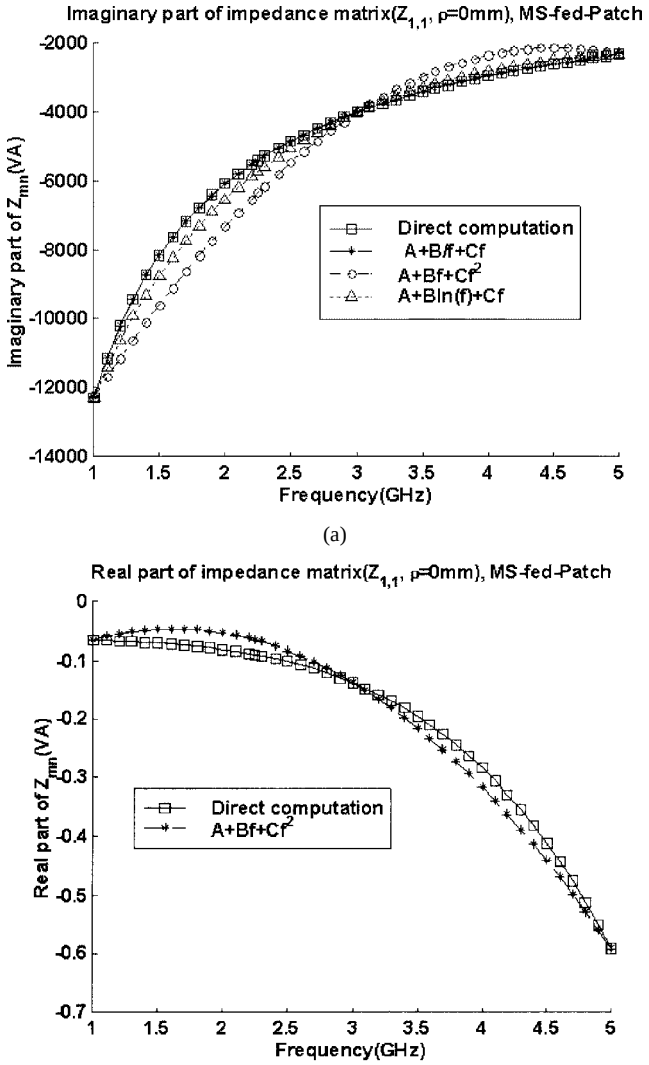

Fig. 3. Comparison of the impedance matrix element derived by using different interpolating functions in the near region ($Z_{1,1}$, $e = 0$ mm). (a) Imaginary part. (b) Real part.

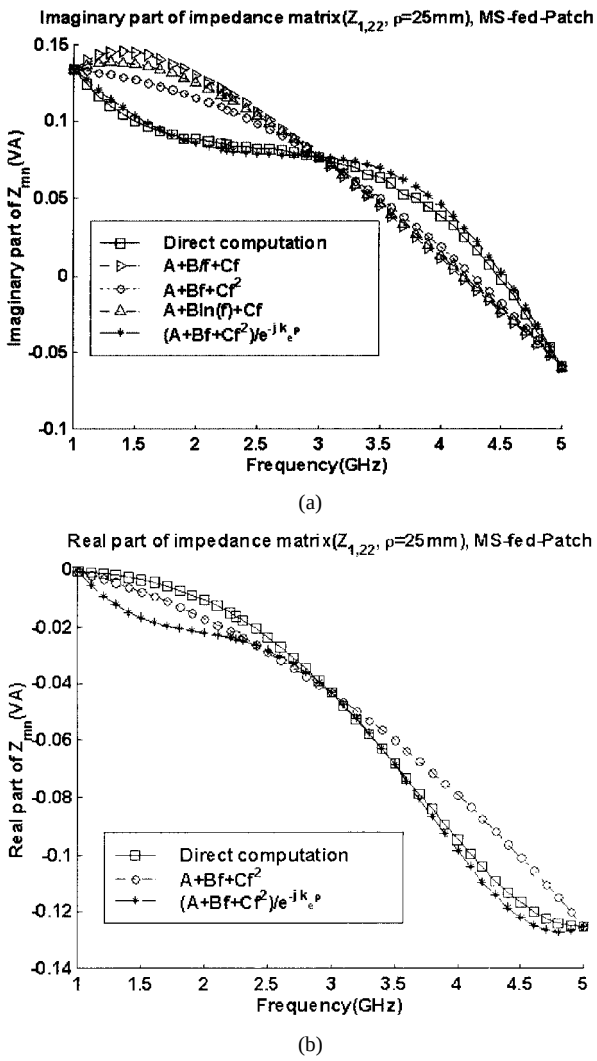

Fig. 4. Comparison of the impedance matrix element derived by using different interpolating functions in the intermediate region ($Z_{1,22}$, $e = 25$ mm). (a) Imaginary part. (b) Real part.

matrices derived at 1, 3, and 5 GHz as the starting points for the interpolation ($\Delta f = 2\,\text{GHz}$). It is evident that the inverse f interpolating function, given in (17), is the most accurate among the three and, hence, is the recommended choice. The results for the real part of the matrix element, for which we use the universal representation for the entire computational domain, are shown in Fig. 3(b) for the near region.

Next, in the intermediate region ($0.45\lambda_e \leq \rho_{mn} \leq 0.75\lambda_e$), we find that the phase variations increase and dominate the frequency variations of the impedance matrix elements. To circumvent this problem, we factor out this term and interpolate only the rest, which is relatively slowly varying, and recover the original impedance matrix elements later by restoring the phase factor to the interpolated result. In this region, we use the quadratic function below for both the real and imaginary parts of $Z_{mn}/e^{-jk_e\rho_{mn}}$ as follows:

$$X(f) = A + Bf + Cf^2. \tag{18}$$

Fig. 4(a) and (b) shows the interpolation results of the element $Z_{1,22}(\rho = 25\text{ mm})$ with and without the removal of the phase factor for both the imaginary and real parts. It is obvious that, in this region, the interpolation works better when the phase factor is removed.

Finally, for the far region ($\rho_{mn} > 0.75\lambda_e$), the influence of the phase term $e^{-jk_e\rho_{mn}}$ becomes more severe and the elements fluctuate more rapidly as functions of the frequency. Similar to the intermediate region, the phase term is again factored out and only the remaining is interpolated. For this region, we use the cubic function below for the imaginary parts of $Z_{mn}/e^{-jk_e\rho_{mn}}$, i.e., we let

$$X(f) = Af + Bf^2 + Cf^3 \tag{19}$$

while the quadratic function is still used for the real parts of $Z_{mn}/e^{-jk_e\rho_{mn}}$. Fig. 5(a) and (b) shows the interpolation results with and without removing the phase factor for both the imaginary and real parts. We see that the interpolation also works better in this region when the phase term is factored out.

To demonstrate the efficacy of the proposed method, we have compared the current coefficients obtained from our interpolation scheme with two others [7], [8] against the results of the

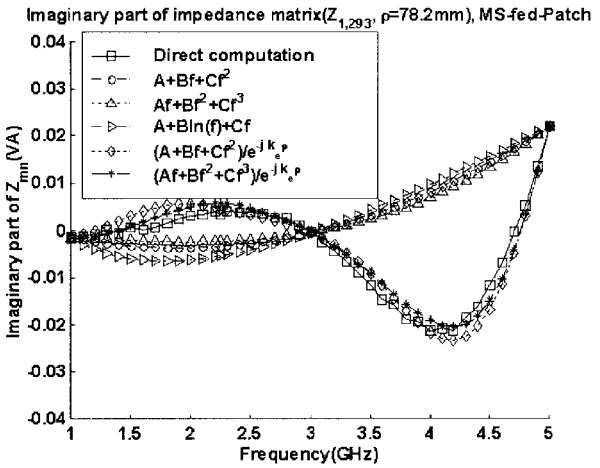

(a)

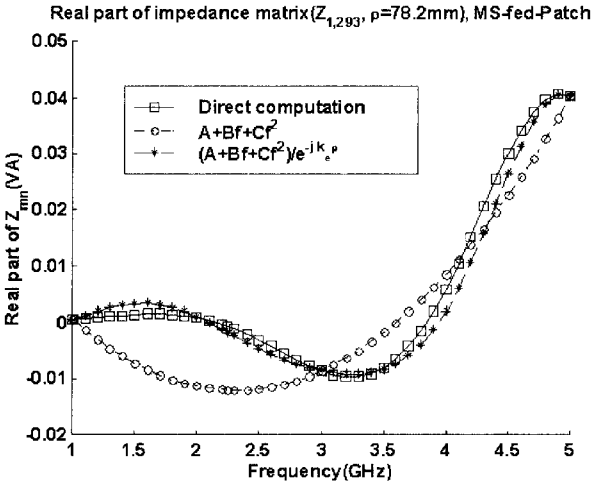

(b)

Fig. 5. Comparison of impedance matrix element derived by using different interpolating functions in the far region ($Z_{1,293}$, $e = 78.2$ mm). (a) Imaginary part. (b) Real part.

direct computation. Three different interpolation schemes including the proposed one are implemented from 1 to 5 GHz for the patch antenna and the error norm for the current coefficients is defined by $e_i = \sqrt{\sum_i |I_i^{\text{inpt}} - I_i^{\text{direct}}|^2} / \sqrt{\sum_i |I_i^{\text{direct}}|^2}$. For the first case, the proposed interpolation scheme is employed. For the second case, we employ the inverse f and quadratic functions for interpolating the imaginary and real parts, respectively, over the entire region. For this case, the distance criterion for factoring out the phase term is $0.5\lambda_e$. For the last case, we experiment with the same interpolating function as above, except for the imposition of the distance criterion of $0.5\lambda_o$. Fig. 6 shows the error norm for the current coefficients for three cases. The results clearly show that the scheme we have proposed works better than the other two existing schemes.

III. Numerical Results and Comparison

The three-region interpolation scheme, described above, has been applied to the matrices for several planar microstrip structures and the results are compared with that of direct computation to assess their accuracies. The examples chosen are: 1) a patch antenna fed by a microstrip line and 2) a 4×4 planar patch array.

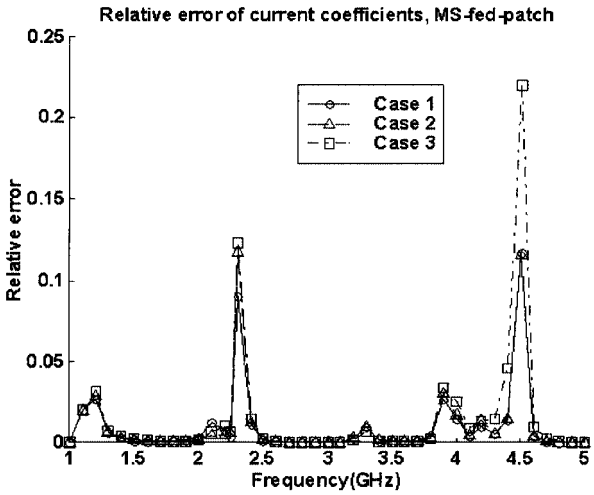

Fig. 6. Comparison of relative errors of current coefficients using different interpolation schemes for the microstrip line-fed patch antenna.

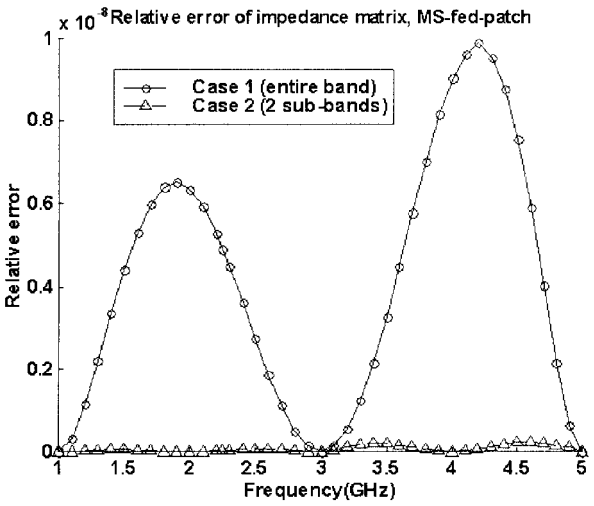

(a)

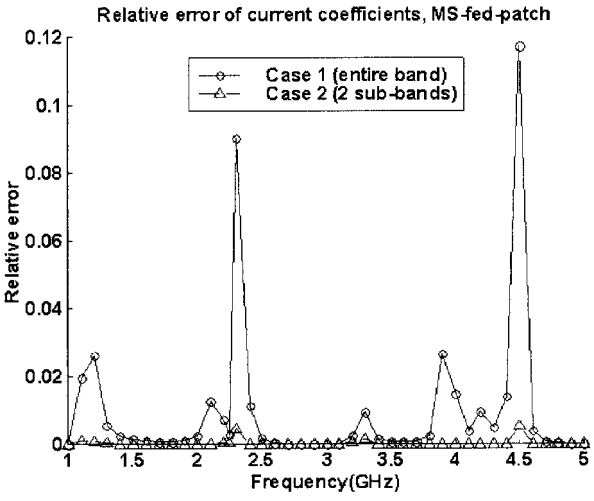

(b)

Fig. 7. Relative errors for the microstirp line-fed patch antenna. (a) Impedance matrix. (b) Current coefficients.

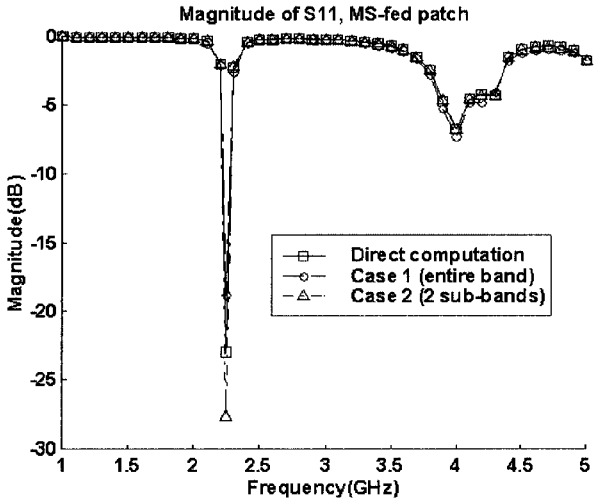

(a)

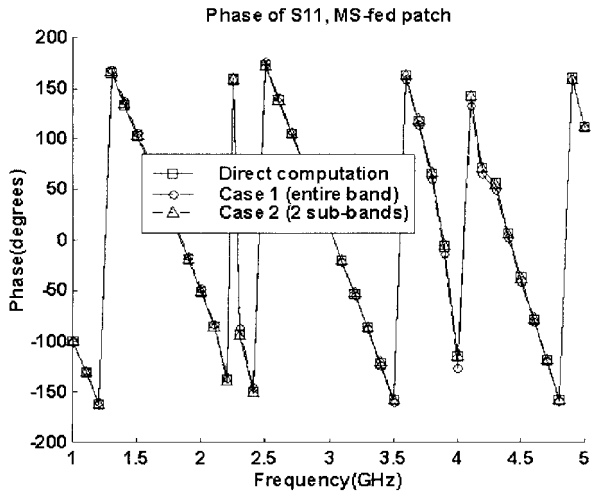

(b)

Fig. 8. Comparison of the $S11$ characteristic for the microstrip line-fed patch.

A. Microstrip Line-Fed Patch Antenna

The first example for the impedance matrix interpolation is a patch antenna, fed by a microstrip line, as shown in Fig. 1. A modeling of this antenna at the highest frequency of 5 GHz with a cell size of 2.5 mm requires 730 unknowns when a uniform rectangular grid and rooftop basis functions are employed, and it remains unchanged over the frequency range of interest. The antenna has the first resonant frequency at 2.25 GHz, while the second one occurs at 4 GHz. The proposed interpolation scheme is implemented from 1 to 5 GHz, and two different frequency step sizes are used for this case. For the first case, the frequency step size $\Delta f = 2$ GHz is employed, and the matrices are directly computed and stored at 1, 3, and 5 GHz. For the second case, we use a frequency step of 1 GHz so that the entire frequency band is divided into two sub-bands, *viz.* 1–3 and 3–5 GHz. The impedance matrices at 1, 2, and 3 GHz are precalculated directly for the first sub-band, while matrices at 3, 4, and 5 GHz are precalculated directly for the second sub-band. The impedance matrix and current coefficients obtained from the proposed interpolation scheme are compared to those of direct computation at every 0.1 GHz including the first resonant frequency at 2.25 GHz, with the error norm for the impedance matrix defined by $e_z = \sqrt{\sum_i \sum_j |Z_{i,j}^{\text{inpt}} - Z_{i,j}^{\text{direct}}|^2} / \sqrt{\sum_i \sum_j |Z_{i,j}^{\text{direct}}|^2}$, as shown in Fig. 7. The $S11$ characteristics and input impedance

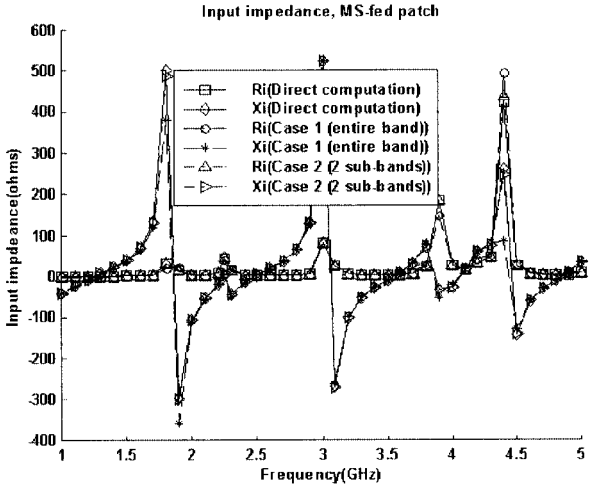

Fig. 9. Comparison of the input impedance response for the microstrip line-fed patch antenna.

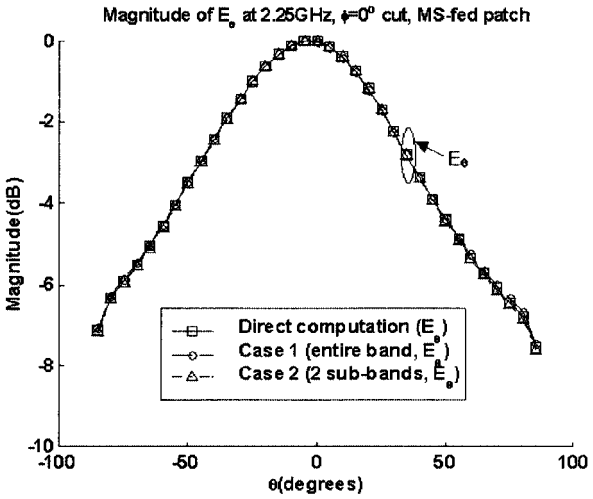

(a)

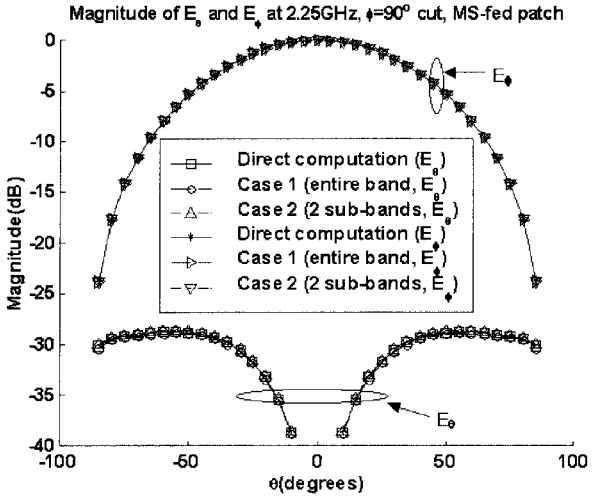

(b)

Fig. 10. Comparison of the radiation patterns at 2.25 GHz for the microstrip line-fed patch. (a) $\phi = 0°$ cut. (b) $\phi = 90°$ cut.

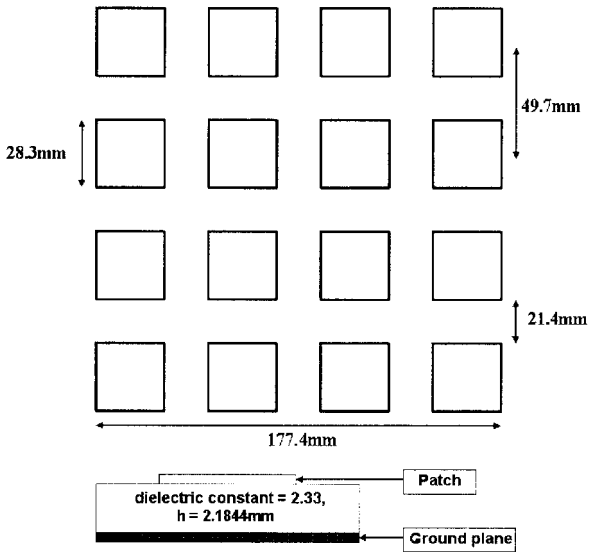

Fig. 11. Geometry of a 4×4 planar square patch array.

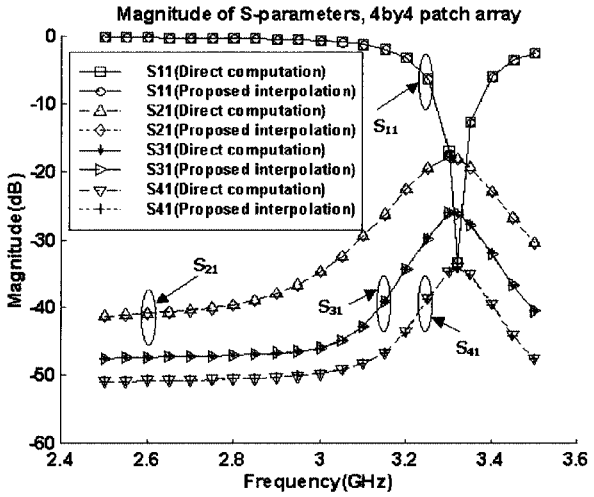

Fig. 12. Comparison of the S-parameters for the 4×4 square patch array.

responses for the two cases are compared in Figs. 8 and 9, while Fig. 10 compares the radiation patterns at 2.25 GHz. We observe that the error norm for the second case, which uses a frequency step size of 1 GHz, is much lower than that for the case where the frequency step size was 2 GHz. At this point, we need to discuss how to choose an optimum interpolation frequency step size [6]. Since we use the effective wavenumber and wavelength, the corresponding wavenumber step size is $\Delta k_e = 2\pi/\lambda_e$. We require the interpolation step size to introduce a phase change of less than π; hence, $\Delta k_e \rho_{mn} \leq \pi$. Let us assume that the largest distance between the source and testing functions as $\rho_{\max}$. From this, we can derive the maximum interpolation step size to be $\Delta f_M = f_H/2(\rho_{\max}/\lambda_e)$, where f_H is the upper limit of the frequency band. It turns out that a frequency step size of less than Δf_M is a good guideline for achieving a close agreement with the results of direct computation. For this example, the largest distance $\rho_{\max}$ is approximately $2.5\lambda_e$ at the highest frequency and Δf_M is approximately 1 GHz. As we observe from Figs. 7–10, the interpolation result with a frequency step size of 1 GHz shows good agreement when compared to the direct computation. The time for the direct impedance matrix calculation is 6.6 s per frequency on a Pentium III PC with a 550-MHz processor and 1-GB RAM, whereas it is 0.42 s using the interpolation scheme on the same machine.

B. 4 × 4 Square Patch Array

The second example considered is a 4×4 planar square patch array with a length of 28.3 mm and a center-to-center separation between the elements of 49.7 mm, as shown in Fig. 11. The individual patches are fed by a strip probe of 1-mm radius and is offset along the y-axis by 5 mm. The substrate thickness is 2.1844 mm and its $\varepsilon_r = 2.33$. The number of unknowns for this problem is 2096, when it is modeled by using the rooftop basis functions. The array has its first resonant frequency at 3.32 GHz, and the interpolation scheme is implemented from 2.5 to 3.5 GHz. The frequency step size of $\Delta f = 0.5$ GHz is used, and the impedance matrices at 2.5, 3, and 3.5 GHz are used for the interpolation. For this example, the largest distance $\rho_{\max}$ between the source and testing functions is approximately $4\lambda_e$ at the highest frequency and Δf_M is approximately 0.45 GHz, which is close to the frequency step size used, for this example. The magnitude of S-parameters are plotted in Fig. 12, and these are computed at every 0.05 GHz including the resonant frequency of 3.32 GHz. The results show good agreement compared to the direct computation result. The direct impedance matrix filling time for each frequency is 43.09 s on a Pentium III PC with 550-MHz processor and 1-GB RAM, while it is 9.42 s per frequency when the proposed interpolation technique is used.

IV. Conclusions

In this paper, we have presented a new interpolation technique for MoM matrices associated with planar microstrip structures. We have identified three different regions, *viz*. near, intermediate, and far, on the basis of the distance between the source and testing functions, and have presented different interpolating schemes tailored for each region. The matrix interpolation scheme is extendable to a general class of problems that are currently under investigation by the authors.

References

[1] R. F. Harrington, *Field Computations by Moment Methods*. New York: McMillan, 1968.

[2] M. I. Aksun and R. Mittra, "Derivation of closed-form Green's functions for a general microstrip geometry," *IEEE Trans. Microwave Theory Tech.*, vol. 40, pp. 2055–2062, Nov. 1992.

[3] I. Park, R. Mittra, and M. I. Aksun, "Numerically efficient analysis of planar microstrip configurations using closed-form Green's functions," *IEEE Trans. Microwave Theory Tech.*, vol. 43, pp. 394–400, Feb. 1995.

[4] J. R. Mosig, "Arbitrarily shaped microstrip structures and their analysis with a mixed potential integral equation," *IEEE Trans. Microwave Theory Tech.*, vol. 36, pp. 314–323, Feb. 1988.

[5] E. H. Newman and D. Forrai, "Scattering from a microstrip patch," *IEEE Trans. Antennas Propagat.*, vol. AP-35, pp. 245–251, Mar. 1987.

[6] E. H. Newman, "Generation of wide-band data from the method of moments by interpolating the impedance matrix," *IEEE Trans. Antennas Propagat.*, vol. 36, pp. 1820–1824, Dec. 1988.

[7] K. Virga and Y. Rahmat-Samii, "Wide-band evaluation of communications antennas using $[Z]$ matrix interpolation with the method of moments," in *Proc. IEEE AP-S Symp.*, vol. 2, June 1995, pp. 1262–1265.

[8] ——, "Efficient wide-band evaluation of mobile communications antennas using $[Z]$ or $[Y]$ matrix interpolation with the method of moments," *IEEE Trans. Antennas Propagat.*, vol. 47, pp. 65–76, Jan. 1999.
[9] A. S. Barlevy and Y. Rahmat-Samii, "An efficient method for wide band characterization of periodic structures using a modified Z matrix interpolation," in *Proc. IEEE AP-S Symp.*, vol. 1, July 1997, pp. 56–59.
[10] ——, "Characterization of electromagnetic band-gaps composed of multiple periodic tripods with interconnecting vias: Concept, analysis, and design," in *IEEE AP-S Symp.*, vol. AP-49, Mar. 2001, pp. 343–353.
[11] J. R. Mosig and F. E. Gardiol, "Analytical and numerical techniques in the Green's function treatment of microstrip antennas and scatterers," *Proc. Inst. Elect. Eng.*, pt. H, vol. 130, pp. 175–182, Mar. 1983.
[12] ——, "General integral equation formulation for microstrip antennas and scatterers," *Proc. Inst. Elect. Eng.*, pt. H, vol. 132, pp. 424–432, Dec. 1985.
[13] Y. L. Chow and W. C. Tang, "3-D Green's functions of microstrip separated into simpler terms—Behavior, mutual interaction and formulas of the terms," *IEEE Trans. Microwave Theory Tech.*, vol. 49, pp. 1483–1491, Aug. 2001.

Junho Yeo (S'01) received the Bachelors degree in electronics engineering and Masters degree in electronics engineering from Kyungpook National University, Daegu, Korea, in 1992 and 1994, respectively, and is currently working toward the Ph.D. degree in electrical engineering at Pennsylvania State University, University Park.

During 1994 and 1999, he was a Researcher with the Republic of Korea Agency for Defense Development (ROKADD), Korea, where he was involved with the development of missile telemetry systems, especially the design and fabrication of low-profile transmitting and ground-station receiving antennas. Since 1999, he has been a Graduate Research Assistant with the Electromagnetic Communication Laboratory, Pennsylvania State University. His research interests include computational electromagnetics, design of conformal fractal antennas and wide-band antennas for wireless applications, genetic algorithm (GA)-based design of artificial magnetic ground planes (AMGs) utilizing FSSs, and development of numerically efficient techniques for the analysis of planar microstrip structures.

Raj Mittra (S'54–M'57–SM'69–F'71–LF'96) is currently a Professor in the Electrical Engineering Department, Pennsylvania State University, University Park. He is also the Director of the Electromagnetic Communication Laboratory, which is affiliated with the Communication and Space Sciences Laboratory of the Electrical Engineering Department, Pennsylvania State University. Prior to joining Pennsylvania State University, he was a Professor of electrical and computer engineering with the University of Illinois at Urbana-Champaign. He is the President of RM Associates, a consulting organization that provides services to industrial and governmental organizations both in the U.S. and abroad. He has authored or coauthored over 600 technical papers and over 30 books or book chapters on various topics related to electromagnetics, antennas, microwaves, and electronic packaging. He holds three patents on communication antennas. He has advised over 80 Ph.D. students, approximately an equal number of M.S. students, and has mentored approximately 50 post-doctoral research associates and visiting scholars at the Electromagnetic Compatibility (EMC) Laboratories at the University of Illinois at Urbana-Champaign and Pennsylvania State University.

Dr. Mittra is Past-President of the IEEE Antennas and Propagation Society (IEEE AP-S) and he has served as the editor of the IEEE TRANSACTIONS ON ANTENNAS AND PROPAGATION. He was the recipient of the 1965 Guggenheim Fellowship Award, the 1984 IEEE Centennial Medal, the 2000 IEEE Millennium Medal, and the 2002 IEEE AP-S Distinguished Achievement Award.